

# Three-dimensional finite element analysis of single-edge cracked low density polyethylene

Min-Diaw Wang, Takeshi Katagiri, Eiji Nakanishi\* and Sadao Hibi

Department of Materials Science and Engineering, Polymer Course, Nagoya Institute of Technology, Nagoya 466, Japan

(Received 25 October 1991; accepted 27 November 1991)

Three-dimensional finite element (3-D FEM) analysis has been performed on single-edge cracked low density polyethylene to investigate the fracture mechanics for the stationary and growing crack. Input of the mechanical behaviour to the FEM calculation is derived from the uncracked specimen. It is found that, without referring to either the plastic flow theory or to the plastic deformation theory, the 3-D FEM analysis predicts the load-displacement curve of the cracked samples, the crack extension to the applied stress curve and the development of the plastic zone to acceptable agreement with the experimental results. Both the stress and strain at the crack tip are three-dimensional while those remote from the crack tip are close to the two-dimensional state.

(Keywords: 3-D FEM analysis; single-edge cracked tension; low density polyethylene; crack tip singularity; plastic zone; fracture)

## INTRODUCTION

Fracture mechanics is not only an interesting topic in mechanics but also an important field for research of materials, and it has received worldwide attention for several decades. After Rice<sup>1</sup> reported the  $J$ -integral theory, research work has been directed to using this theory in analysing crack tip stress and strain phenomena. Hutchinson<sup>2</sup> and Rice and Rosengren<sup>3</sup> proposed the HRR phenomenon, which was based on either plane strain or plane stress assumption. The HRR phenomenon, which is dominated by a single value, the  $J$ -integral, is shown in the following equation:

$$\sigma_{ij} \sim \sigma_0 \left[ \frac{J}{\sigma_0 \epsilon_0 I_n r} \right]^{1/n+1} \sigma_{ij}(\theta, n) \quad (1)$$

As the  $J$ -integral was originally developed for two-dimensional plane strain, its application to ductile material, which is characterized by difficulty in meeting the plane strain criterion, deserves more study. Schmitt and Kienzler<sup>4</sup> modified this theory by concerning the stress work density and an additional volume integral in the  $J$  theory was derived. Schmitt and Kienzler also suggested that, for a growing crack under plastic collapse conditions, the stress or strain state at the crack tip should be a result of crack extension rather than being the criterion that controlled the fracture process. Dodds *et al.*<sup>5</sup> compared the  $J_{SSY}$  ( $J$ -integral under small scale assumption) with the  $J_{SENB}$  ( $J$ -integral from single-edge notched bending) using finite element (FEM) analysis and concluded that the ASTM E 813-87 criterion is not adequate in fulfilling the small scale yielding condition. They suggested the following requirement:

$$Bba \geq 200J_{IC}/\sigma_{flow} \quad (2)$$

where  $B$  is the thickness,  $b$  is the ligament length,  $a$  is

the crack length,  $J_{IC}$  is the integral at crack initiation and  $\sigma_{flow}$  is the flow stress. The stress state at the crack tip is also studied while deviation of the calculation from the HRR phenomenon is observed. This is not surprising since many other researchers obtained similar results<sup>6-8</sup>. Dodds *et al.* also performed curve fitting upon the calculation. Their result showed that the stress is still an exponential function of  $r$  (the distance from the crack tip) while the exponent is related to the strain hardening index.

As applications involving composite materials using polymer as the matrix have become more important, research of their fracture has also received wider attention. While ductile polymers show non-linear mechanical behaviour, the fracture of these types of material deserves more study. In tensile testing, one can observe that the tangent of the unloading curve is quite different from that of the loading curve. This implies that the assumption that polymeric materials show proportional plastic deformation is questionable. As crack propagation is accompanied by elastic unloading<sup>9</sup>, the stress and strain at the crack tip may differ from predictions using theories with a single dominant  $J$ -integral. In order to study the stress and strain state of cracked polymer materials, three-dimensional FEM is performed and the calculation is compared with experimental data from low density polyethylene (LDPE).

## FINITE ELEMENT ANALYSIS

The construction of the elements is shown in *Figure 1*. Due to the symmetry to the crack plane, only the upper half is shown here. The elements surrounding the crack tip are finely divided. The system is displacement-controlled, that is, the upper bound is set to be fixed while the lower bound will move downwards by a

\*To whom correspondence should be addressed

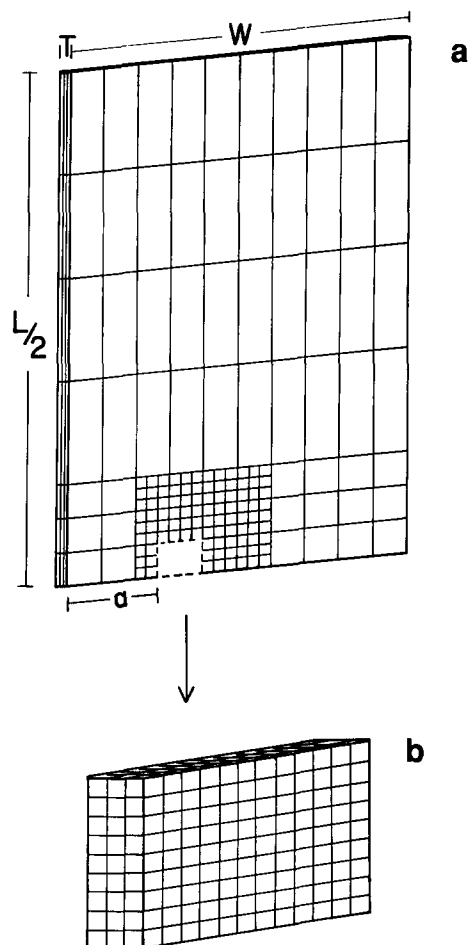


**Figure 1** Finite element mesh of the specimen. Elements inside the dashed line of (a) are magnified in (b).  $L = 90$  mm,  $W = 30$  mm,  $T = 1$  mm

predetermined amount during each calculating stage. The mechanical properties, including the stress-strain relationship and yielding, are derived from tensile tests on uncracked specimens. The stiffness matrix is checked before executing each stage and modified by the result from the previous stage. This modification is based on the real experimental data without assuming any deformation theory. The Poisson ratio is set to be 0.45 although this value is not really constant during the experiment. This does not significantly affect the calculated results because the value of the Poisson ratio has a very small effect on the resultant stress. The crack lengths are set to be 9, 12, 15, 18 and 21 mm, which correspond to  $a_0/w$  ratios (initial crack length to width ratio) from 0.3 to 0.7. Propagation of the crack is controlled by a self-checking command so that if the stress of any element becomes larger than the material strength, that element will be taken out in the next stage. It is found that, assuming isotropism, a crack only propagates in the crack plane.

#### EXPERIMENTAL

LDPE was supplied by the Mitsubishi Petro. Chem. Co. Ltd (trade no. PK-30). Sheets of 1 mm thickness were made by melt pressing at 200°C. No planar orientation was confirmed by the uniform rings from wide angle X-ray diffraction pictures. Test specimens were then cut with the following dimensions: length, 90 mm; width,

30 mm; initial crack length, 9–21 mm (see *Figure 1*). The length to width ratio was designed to be 3 so that the chuck effect can be neglected, as shown by our previous work<sup>10</sup>. The tensile speed was set at 0.4 mm min<sup>-1</sup> for both uncracked and cracked specimens using Tensilon UTM-4LH. Evaluation of the plastic zone and energy analysis were as described in previous work<sup>11,12</sup>. Crack growth was monitored by a camera.

#### RESULTS AND DISCUSSION

The stress-displacement curves from FEM calculation, derived from the average stress of the boundary elements, are shown in *Figure 2* with experimental data for comparison. Basically the calculation is consistent with the experimental result. Specimens with initial crack length,  $a_0 = 21$  mm, show deviation from the calculation at large displacement. *Figure 3* shows the graph of crack extension versus stress. Again, FEM calculation is in good agreement with the experimental results. Specimens with  $a_0 = 21$  mm show a faster crack growth rate than predicted. From experiment, it was found that specimens with  $a_0 = 21$  mm showed extremely large extension at the crack tip while, at the end of the ligament, deflection was observed. This is partly due to the ductile property of LDPE and partly due to free rotation of the upper chuck. From *Figures 2* and *3*, the FEM analysis in this study is limited to the ratio  $a_0/w < 0.7$ . Crack opening displacement observed from experiment is much larger than that calculated. Even though FEM is only a simulation method, it can be used to study phenomena

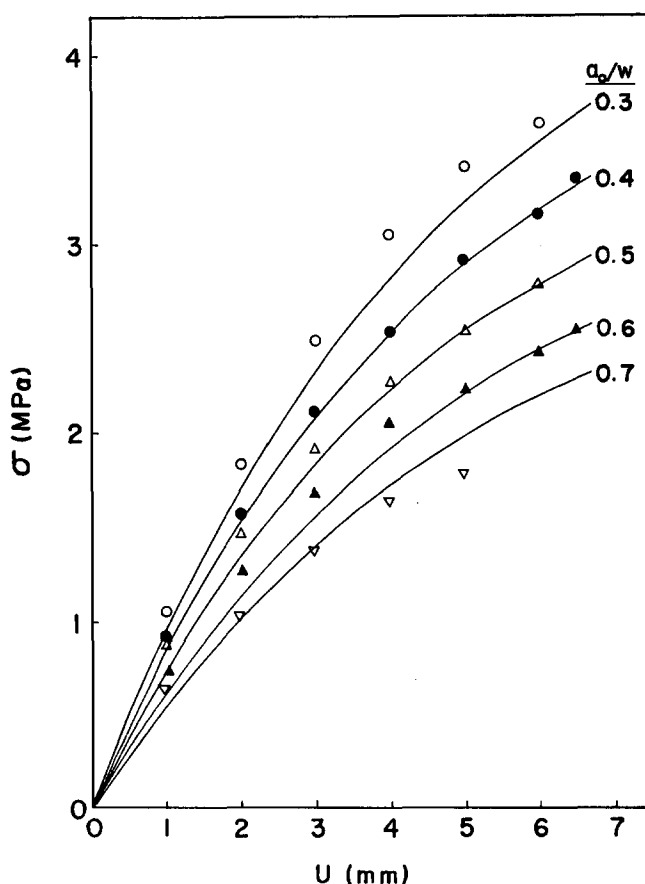


**Figure 2** Comparison of the stress versus displacement curves of the FEM calculation with experimental results. Symbols represent experimental results  $a_0$  (mm):  $\circ$ , 9;  $\bullet$ , 12;  $\triangle$ , 15;  $\blacktriangle$ , 18;  $\nabla$ , 21

that cannot be observed from experiment. From the agreement of Figures 2 and 3, we feel it is acceptable to use the FEM result to interpret the stress state in the real specimen. Figures 4a and b show the stresses parallel to and perpendicular to the loading direction in the crack plane, respectively, with 1.35 MPa remote stress applied at the chuck. It can be seen that the stress level changes

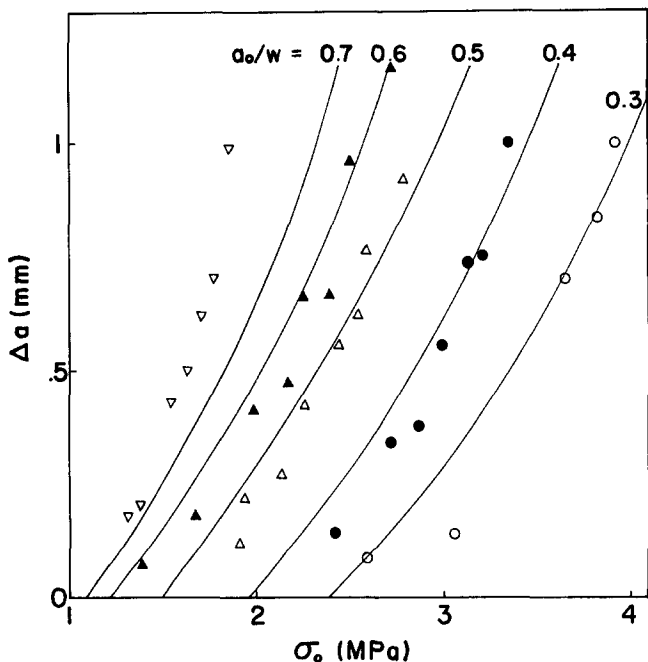


Figure 3 Comparison of the crack growth  $\Delta a$  versus  $\sigma_0$  of the FEM calculation with experimental results. Symbols represent experimental results and have the same meaning as in Figure 2

with the  $a_0/w$  ratio. It is interesting to note that, at large values of  $r$  (distance from crack tip), the relationship between the stress and the initial crack length, as shown in equation (3), is quite close to that predicted by linear fracture mechanics:

$$\sigma = \frac{\sigma_0}{\sqrt{2}} \sqrt{\frac{a}{r}} f(\theta) \quad (3)$$

As the crack tip is approached, the increase of stress intensity for larger  $a_0$  is higher than that for smaller  $a_0$ . Basically, the full stress curve does not correspond to any simple relation of some exponent of  $r$ . This phenomenon is the same for both the centre and the outer part. The stress in the thickness direction,  $\sigma_{zz}$ , shows quite different behaviour. At the crack tip,  $\sigma_{zz}$  is about the same order as  $\sigma_{yy}$  and  $\sigma_{xx}$  and is also  $a_0$ -dependent, but it reduces to almost zero at slightly larger  $r$ . This is quite similar to the results of Nakamura and Parks<sup>13</sup>. Apart from the vicinity of the crack tip, the whole system is close to the generalized plane stress. In linear fracture mechanics, the relationship between the stress and  $r$  for particular values of  $a_0$  and  $\theta$  is only affected by the remote stress  $\sigma_0$ , as shown in equation (3). Quite a different result is obtained from our calculation. Figure 5 shows  $\sigma_{yy}$  normalized by  $\sigma_0$  versus  $r$  with  $a_0 = 15$  mm at different stages. It can be seen that the stress intensity at the crack tip becomes smaller at higher stages, i.e. larger  $\sigma_0$ . This is due to the non-linear behaviour of LDPE. At large  $r$ , where the stress of the elements is lower than the yield stress, the normalized stress becomes almost the same for different stages. Points in Figure 5 are plotted by assuming the following

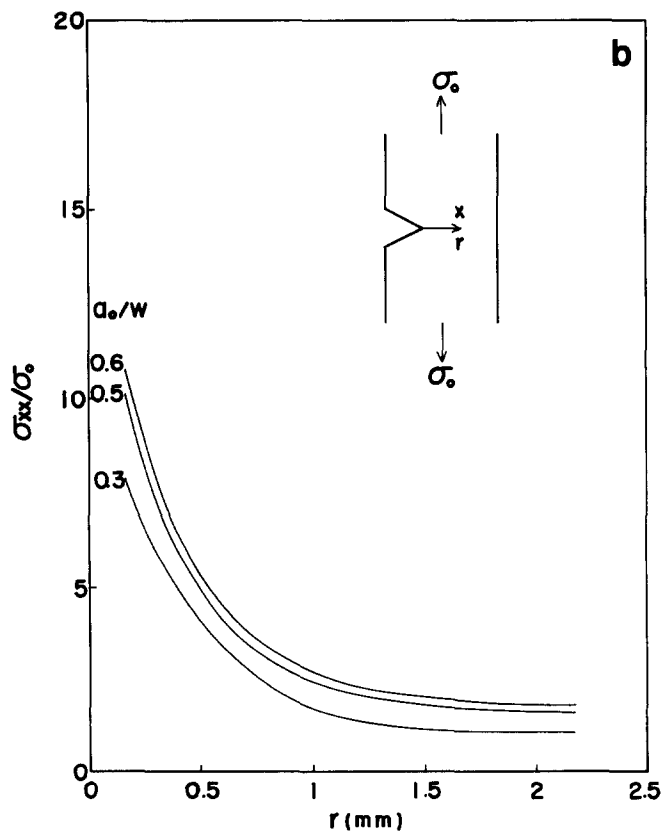
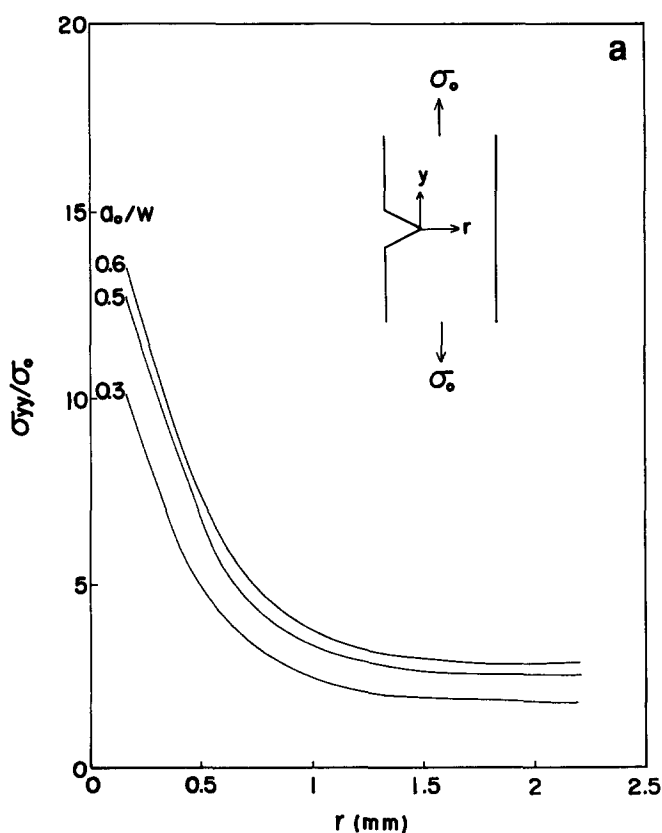


Figure 4 Stress ( $\sigma_{yy}$ ) normalized by the remote stress ( $\sigma_0$ ) versus the distance from the crack ( $r$ ) in the crack plane from FEM calculation with three different  $a_0/w$  ratios. (a) Stress in the load direction ( $\sigma_{yy}/\sigma_0$ ) versus  $r$ ; (b) stress in the ligament direction ( $\sigma_{xx}/\sigma_0$ ) versus  $r$ .  $\sigma_0 = 1.35$  MPa

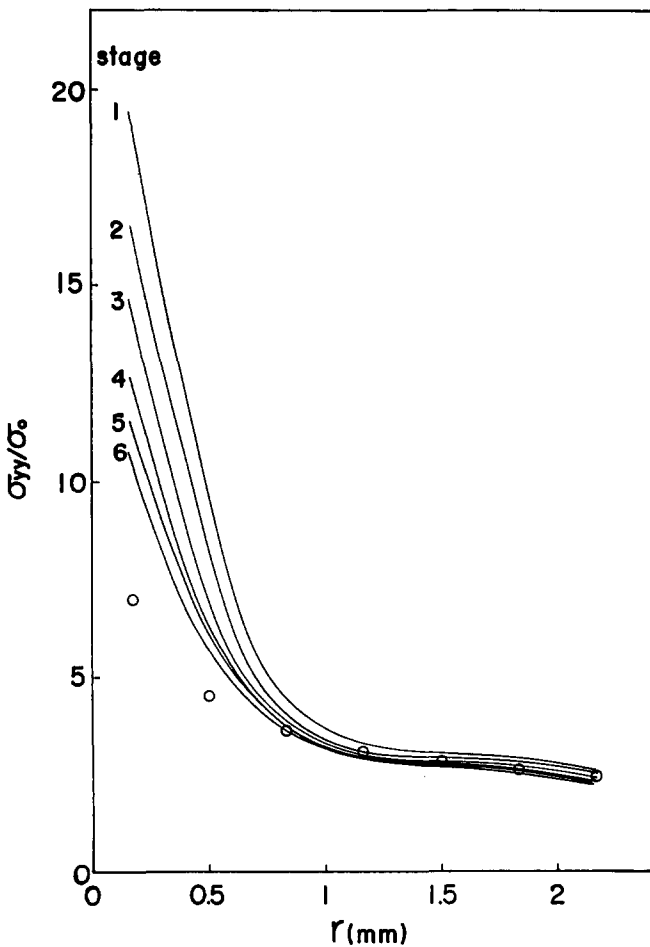


Figure 5 Normalized stress ( $\sigma_{yy}/\sigma_0$ ) versus  $r$  at different stages of FEM calculation. Symbols ( $\circ$ ) represent simulation from equation (4)

relationship:

$$\sigma_{yy}/\sigma_0 \cong Kr^{-1/n+1} \quad (4)$$

where  $K$  is a constant and  $n$  is the strain hardening index, which is 1.52 for the LDPE used in this study. Equation (4) is in good agreement with the calculation except in the vicinity of the crack tip. This agreement is the reason why the plastic zone can be evaluated by a model proposed by Wang *et al.*<sup>11</sup> and will be discussed in detail later.

Assuming that generalized plane stress can be applied to the whole system, we are able to calculate the difference of the principal stress ( $\sigma_1 - \sigma_2$ ). Figures 6a-c show the constant ( $\sigma_1 - \sigma_2$ ) isochromatic fringe loops at different  $\sigma_0$  values. Because the whole system is symmetric according to the crack plane, only plots of the upper half are shown here. It is confirmed that the stress did not show discontinuity for the boundary elements between the finely divided area and the coarsely divided area. As the  $\sigma_0$  values increase, the loop with a particular ( $\sigma_1 - \sigma_2$ ) value moves away from the crack tip and loops with higher ( $\sigma_1 - \sigma_2$ ) values appear. This is quite similar to observations in the experiment. Inside the plastic zone, higher ( $\sigma_1 - \sigma_2$ ) values are obtained. Whether the photoelasticity is still valid in the yielded state is unknown; direct comparison of the iso-( $\sigma_1 - \sigma_2$ ) loops outside and inside the plastic zone could be misleading. Figure 6d is the experimental result with a  $\sigma_0$  value similar to that of Figure 6b. Numbers on the curves are

approximate ( $\sigma_1 - \sigma_2$ ) values derived by the following procedure.

Specimens without a crack are stretched and polarizer and analyser are applied so that the iso-( $\sigma_1 - \sigma_2$ ) fringes can be observed. If the strain is small, it is reasonable to assume that the stress of the specimen is two-dimensional, neglecting the stress in the thickness direction. Therefore, the following equation is approximately valid:

$$\text{at small strain } (\sigma_{yy} - \sigma_{xx})^2 + 3\tau_{xy}^2 = \sigma_e^2 \quad (5)$$

In the middle of the specimen, the shear stress should be zero due to the symmetrical geometry. The principal stresses  $\sigma_1$  and  $\sigma_2$  are then equal to  $\sigma_{yy}$  and  $\sigma_{xx}$ , respectively. Then, equation (5) can be rewritten as:

$$\text{at the middle } (\sigma_1 - \sigma_2)^2 = (\sigma_{yy} - \sigma_{xx})^2 = \sigma_e^2 \quad (6)$$

During the test, different colours appear due to photoelasticity phenomena. The stress when a particular colour reaches the middle of the test specimen is recorded. The same colour appears repeatedly at different stress levels so that a relationship between its sequence of appearance and the stress level can be established. From the colour and the sequence, the retardation,  $R$ , can be determined from the Michel-L'evy chart. Then the photoelasticity stress sensitivity  $\alpha$  can be derived by the following relation:

$$\frac{R}{\lambda_0} = \alpha B |\sigma_1 - \sigma_2| \quad (7)$$

where  $B$  is the thickness of the specimen and  $\lambda_0$  is the wavelength of the particular colour. By this method, the relation between  $\alpha$  and the sequence can be established. This relation is then used to derive the ( $\sigma_1 - \sigma_2$ ) values in Figure 6d using equation (7), through knowledge of the sequence of the particular colour. In this work, we use the colour green, with wavelength = 527  $\mu\text{m}$ , as the particular colour in deriving the ( $\sigma_1 - \sigma_2$ ) values. The above statement is based on the assumption that small strain is maintained so that equations (4)-(7) are valid. We calculate the  $\alpha$  value to the fourth time that the middle position of the specimen turns green and no further. The maximum strain is about 8%. Consistency between Figures 6d and 6b is quite encouraging. In Figure 6d, it can be seen that, inside the plastic zone, the shape of the isochromatic loops is quite different from that outside the plastic zone.

In linear fracture mechanics the equivalent stress,  $\sigma_e$ , can be expressed as a function of  $r$  and  $\theta$  (the angle from the crack plane). In the case of plane strain, a plot of  $\sigma_e$  resembles a pair of leaves, while in the case of plane stress, a plot of  $\sigma_e$  is a circle. From experiments, no information about  $\sigma_e$  in the specimen can be derived, therefore FEM calculation is used to simulate this. Figures 7a-c show the  $\sigma_e$  plot which corresponds to the conditions of Figure 6. At the crack vicinity, the plot of  $\sigma_e$  is close to a circle. As the distance from the crack tip increases, the iso- $\sigma_e$  loop extends more in the loading direction than in the ligament direction. Its shape is between the shapes of plane stress and plane strain. Inside the plastic zone,  $\sigma_e$  plots, which are not shown here, are circular and extremely finely divided. The plastic-elastic boundary and the plastic zone shape can be defined using such plots as shown in Figure 6 by matching the  $\sigma_e$  with the yield stress.

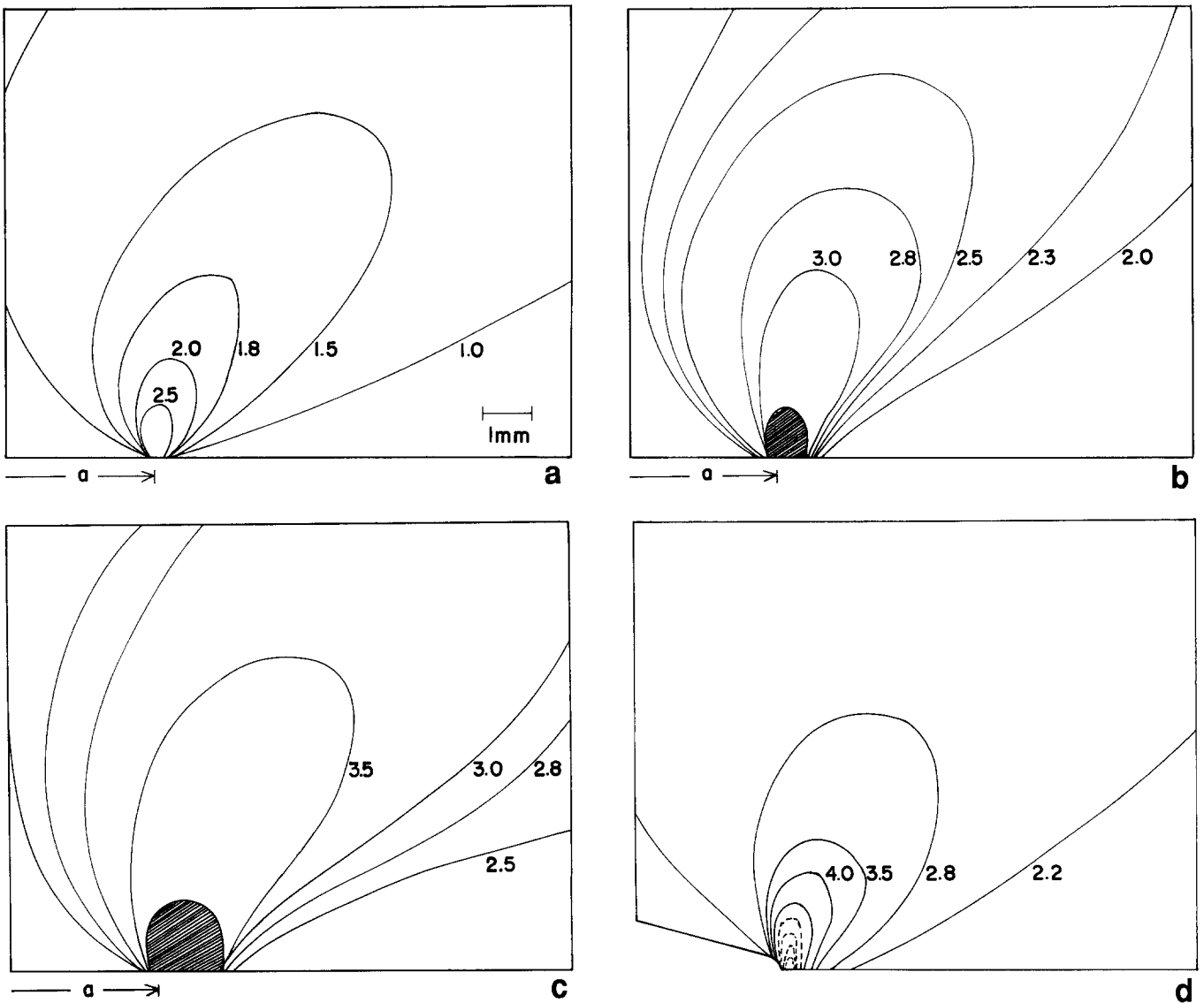


**Figure 6** Plots of the principal stress difference ( $\sigma_1 - \sigma_2$ ) with different  $\sigma_0$  values.  $\sigma_0$  (MPa): (a) 0.747; (b) 1.351; (c) 1.836. (a)–(c) FEM simulation; shaded area is the yielded area. (d) Experimental results with similar conditions to (b); dashed lines represents the plastic zone. Numbers on the curves denote ( $\sigma_1 - \sigma_2$ ) values

Wang *et al.*<sup>11</sup> proposed a model to predict the size of the plastic zone in the crack plane. Basically, this model is derived by modifying the Dugdale model<sup>14</sup> by replacing the constant yield stress inside the plastic zone with a stress function similar to that of equation (4). It is shown as follows:

$$\sigma_\infty \sqrt{\pi(a+r_p)} = \int_a^{a+r_p} \frac{\sigma_Y r_p^{1/n+1}}{\sqrt{\pi(a+r_p)}} \frac{2(\xi-a)^{-1/n+1}}{\sqrt{1-[\xi/(a+r_p)]^2}} \times f(\xi/a+r_p) d\xi \quad (8)$$

where  $\sigma_Y$  is the yield stress and  $\xi$  denotes the distance in the ligament direction. Using this model, the plastic zone size  $r_p$  can be calculated if four other parameters are known:  $\sigma_0$ ,  $a_0$ ,  $n$  and  $\sigma_Y$ , which are predetermined values. As discussed earlier, the stress in the crack plane is not the same as the HRR phenomenon. Equation (4) is valid only at  $r$  values greater than a certain amount. The question arises whether equation (8) is still a good approximation. It is found that changing the stress in the vicinity of the crack tip does not greatly affect the calculation of  $r_p$  because at the crack tip the  $(\xi - a)$  value is very small. Therefore, as long as the relation of equation

(4) is valid for most of the plastic zone, equation (8) can still be used to predict the  $r_p$  value. *Figure 8* shows the results calculated using equation (8) and FEM. The three solid curves in the graph represent perfect plastic, LDPE and perfect elastic conditions. It is found that, at small  $\sigma_0$ , FEM results deviate from equation (4). This is due to the large deviation of the stress state from the stress calculated from equation (4). This can be confirmed from *Figure 5*, which shows a large difference between the FEM result and equation (4) at the early stage. This deviation between FEM results and calculation from equation (8) becomes less significant as  $\sigma_0$  increases. That is, the effect from the inconsistency of the stress and equation (4) is smaller. This can again be referred to *Figure 5* for the later stage. Equation (8) is still a useful tool in approximating the plastic zone even though it is not perfectly correct theoretically.

One more important area in the study of fracture of materials is energy analysis. In elastic-plastic fracture mechanics, this is mostly represented by the  $J$ -integral theory. The critical energy for crack initiation is  $J_{IC}$ , while stable crack growth is related to energy by the  $R$ -curve. Two other theories have been proposed by

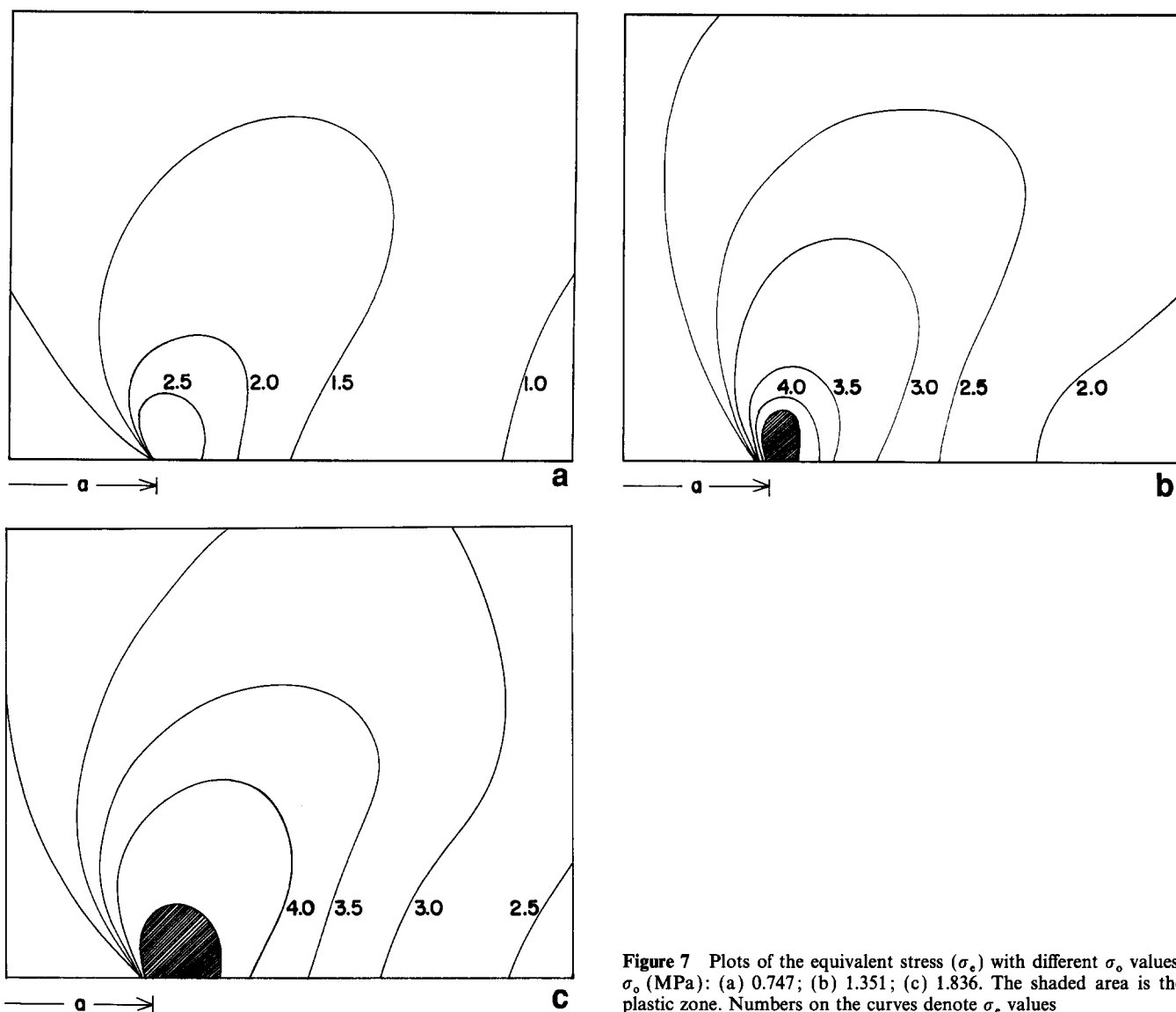


Figure 7 Plots of the equivalent stress ( $\sigma_e$ ) with different  $\sigma_0$  values.  $\sigma_0$  (MPa): (a) 0.747; (b) 1.351; (c) 1.836. The shaded area is the plastic zone. Numbers on the curves denote  $\sigma_e$  values

Andrews<sup>15</sup> and Cotterell and Reddel<sup>16</sup>; they have been discussed by Wang *et al.*<sup>12</sup>, according to whom the crack initiation energy for LDPE used in this study is  $1.4 \text{ kJ m}^{-2}$  using a loading-unloading method. Wang *et al.* also used Andrews' method and obtained  $1.36 \text{ kJ m}^{-2}$  for the crack initiation. Recently, Kim and Joe<sup>17</sup> proposed an experimental method to evaluate the  $J_{IC}$  value of polyetherimide. Their method, unlike that proposed by Begley and Landes<sup>18</sup> which considered all the area under the load-displacement curve as the energy used to drive the crack, is basically similar to Andrews' generalized fracture mechanics<sup>15</sup>. As an unloading curve is not available from FEM results, Kim and Joe's method will be used to evaluate the crack initiation energy. From Figures 2 and 3 we are able to construct a  $\sigma_0$ -displacement plot for various  $a_0$  values with crack initiation points certified; this is shown in Figure 9. The dashed line represents the start of crack growth. As the thickness of the ligament is constant for all the specimens, we will take the energy per unit thickness as the unit for further calculation. The area circumscribed by the solid line and the dashed line is interpreted as the energy consumed for crack initiation for a particular  $a_0$  value. A plot of the energy versus initial crack length  $a_0$  is shown in Figure 10. Least square linear regression of the data

shows the intercept of the x-axis as 30.8 mm and the tangent as  $-1.05 \text{ kJ m}^{-2}$ . While the width of the specimen is 30 mm, initial crack length of 30 mm implies that zero energy is consumed for crack growth. The deviation of 30.8 mm from 30 mm is acceptable. The negative sign of the tangent is equivalent to  $-dU/B da$  which, in turn, equals  $dU/B db$ . This representation is the same as Wang's<sup>12</sup>. Due to the non-linear mechanical behaviour of LDPE, we feel wary of referring this  $1.05 \text{ kJ m}^{-2}$  to the  $J_{IC}$  value; we interpret it as the energy for crack initiation based on the ligament area. The consistency of this value with that of Wang<sup>12</sup> ( $1.4 \text{ kJ m}^{-2}$ ) and that from generalized fracture mechanics ( $1.36 \text{ kJ m}^{-2}$ ) is encouraging. The FEM analysis is thus capable of simulating the fracture energy.

### CONCLUSION

The non-linear behaviour of polymer initiates many difficulties in research of polymer mechanical properties. In this work, direct application of the stress-strain relation of uncracked specimens to FEM calculation, without assuming any deformation theory, yields acceptable results. The stress-displacement curves, the crack growth, the plastic zone and the energy analysis

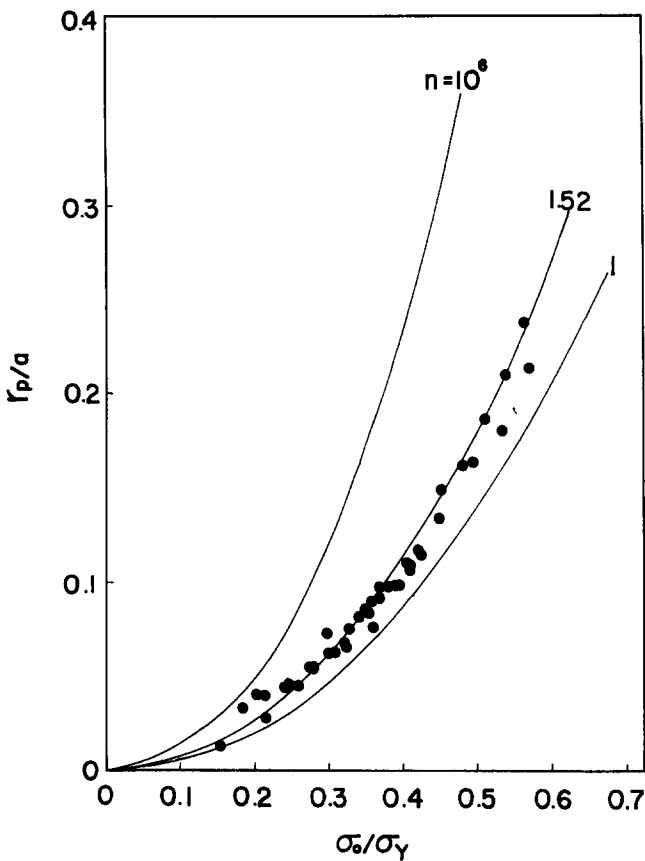


Figure 8 Plot of normalized plastic zone with the crack length ( $r_p/a$ ) versus the normalized remote stress with the yield stress ( $\sigma_0/\sigma_Y$ ). Symbols represent results from FEM calculation. The curves are from equation (8) with three strain hardening indices: perfect plastic ( $n = 10^6$ ), LDPE ( $n = 1.52$ ) and perfect elastic ( $n = 1$ )

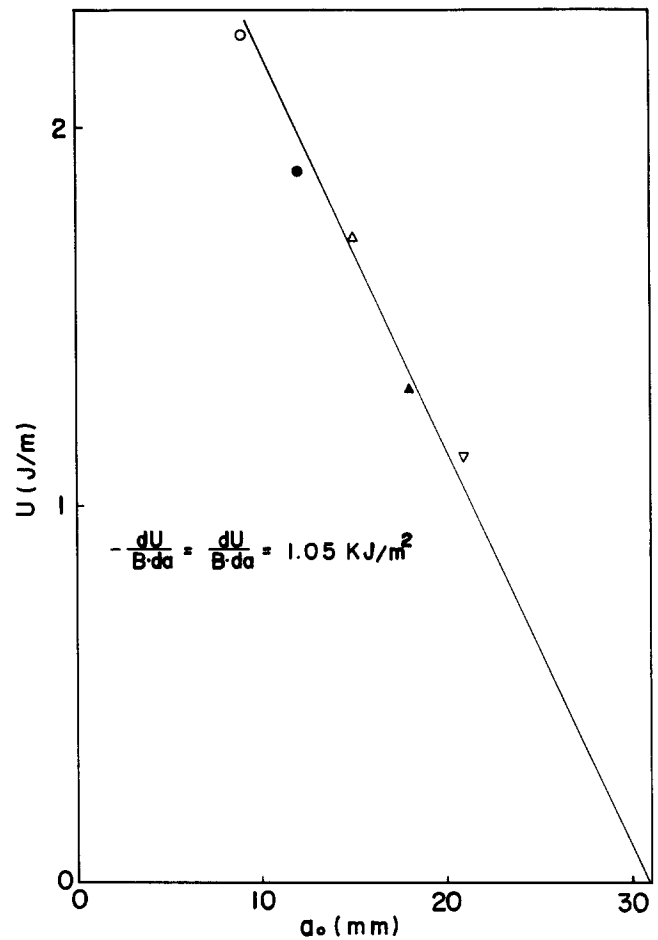


Figure 10 The energy for crack initiation of different  $a_0$  per unit thickness versus the initial crack length. Symbols represent different  $a_0$  values as given in Figure 2

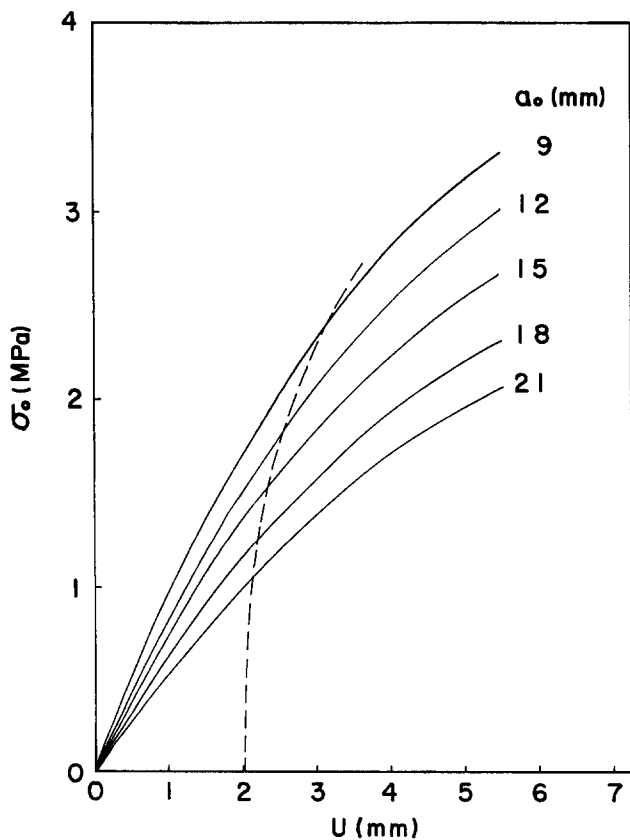


Figure 9 Plot of stress versus displacement from FEM calculation. The dashed line indicates the start of crack growth

of cracked specimens can be simulated. Based on this consistency between FEM calculation and experimental results, the stress state inside the specimen can be understood. The stress at the crack tip is three-dimensional. It decreases as  $r$  increases and, strictly speaking, is not proportional to a simple exponential function of  $r$ . The stress in the thickness direction is only important in the vicinity of the crack tip. For most of the specimen, a state between plane stress and plane strain exists. As the remote stress,  $\sigma_0$ , increases, the stress intensity at the crack tip decreases and the stress becomes closer to an exponential function of  $r$ . This is not expected from traditional linear elastic fracture mechanics.

REFERENCES

- 1 Rice, J. R. *J. Appl. Mech.* 1968, **35**, 379
- 2 Hutchinson, J. W. *J. Mech. Phys. Solids* 1968, **16**, 13
- 3 Rice, J. R. and Rosengren, G. F. *J. Mech. Phys. Solids* 1968, **16**, 1
- 4 Schmitt, W. and Kienzler, R. *Eng. Fract. Mech.* 1989, **32**, 409
- 5 Dodds, R. H. Jr, Anderson, T. L. and Kirk, M. T. *Int. J. Fract.* 1991, **48**, 1
- 6 Shih, C. F. and German, M. D. *Int. J. Fract.* 1981, **17**, 27
- 7 Anderson, T. L. *Int. J. Fract.* 1989, **41**, 79
- 8 Nakamura, T. and Parks, D. M. *J. Mech. Phys. Solids* 1990, **38**, 787
- 9 Hutchinson, J. W. and Paris, P. C. in 'Elastic-Plastic Fracture', ASTM, STP 668, 1979, 37
- 10 Amano, M., Wang, M., Hibi, S., Mori, T. and Kadota, M. *Kobunshi Ronbunshu* 1990, **47**, 537

*3-D finite element analysis: M.-D. Wang et al.*

- |    |   |    |   |
|----|---|----|---|
| 11 | Wang, M., Nakanishi, E., Hashizume, Y. and Hibi, S. <i>Polymer</i> 1992, <b>33</b> , 2715 | 14 | Dugdale, D. S. <i>J. Mech. Phys. Solids</i> 1960, <b>8</b> , 100                |
| 12 | Wang, M., Nakanishi, E., Hashizume, Y. and Hibi, S. <i>Polymer</i> in press               | 15 | Andrews, E. H. <i>J. Mater. Sci.</i> 1974, <b>9</b> , 887                       |
| 13 | Nakamura, T. and Parks, D. M. <i>J. Mech. Phys. Solids</i> 1990, <b>38</b> , 787          | 16 | Cotterell, B. and Reddel, J. K. <i>Int. J. Fract.</i> 1977, <b>13</b> , 267     |
|    |   | 17 | Kim, B. H. and Joe, C. R. <i>Eng. Fract. Mech.</i> 1989, <b>34</b> , 221        |
|    |   | 18 | Begley, J. A. and Landes, J. D. in 'Fracture Toughness', ASTM, STP 514, 1972, 1 |